Methane Activation by Laser-Ablated Group 3 Metal Atoms: Infrared Spectra and Structures of the CH_3-MH and CH_2-MH_2 Complexes

Han-Gook Cho and Lester Andrews*

Department of Chemistry, University of Incheon, 177 Dohwa-dong, Nam-ku, Incheon, 402-749, South Korea, and Department of Chemistry, University of Virginia, P.O. Box 400319, Charlottesville, Virginia 22904-4319

Received September 6, 2006

Methane activation reactions with group 3 metal atoms find that Sc, Y, and La are just as effective as other early transition metals. Two primary products, CH_3-MH and CH_2-MH_2, are identified for each metal from the matrix IR spectra. The single insertion product becomes more favorable with increasing atomic mass of the metal, opposite the general trend observed from other early transition metal systems. The C−M bond lengths of CH_3-MH and CH_2-MH_2 are comparable to each other, on the basis of electronic structure calculations, and the methylidene dihydride complex is symmetrical without agostic distortion. The number of valence electrons of the metal is evidently an important factor in the magnitude of the agostic interaction in these simple methylidene systems.

Introduction

Reactions of laser-ablated group 4, 5, and 6 transition metal atoms with methane and methyl halides have recently generated new class of small insertion products and high-oxidation-state complexes with multiple carbon−metal bonds.[1−7] They provide good model systems to study the effects of ligands and substituent modifications for much larger high-oxidation-state transition metal complexes, which have important catalytic properties for metathesis reactions of alkenes, alkynes, and cyclic compounds.[8] The new products often show interesting reactivities, ligand effects, and fascinating photochemistry including persistent photoreversibilities and dramatic product increases.[1−7] The methylidene complexes, the simplest form of alkylidene complexes, are similar to those of the much larger relatives[8] and normally have agostically distorted structures, which feature unequal C−H bond lengths and H−C−M bond angles.

While high-oxidation-state complexes of early transition metals with multiple carbon−metal bonds have been extensively studied, stable alkylidene complexes of group 4 metals are rare and such complexes for group 3 metals have not been reported.[8] Reactions of group 3 metals with small alkanes have not been studied often. Sunderlin and Armentrout have investigated reactions of group 3 metal cations with CH_4 and C_2H_6 using guided ion beam mass spectrometry and found that MCH_2^+, $MC_2H_2^+$, and $MC_2H_4^+$ were the major products.[9] Freiser et al. performed gas-phase reactions of Y^+ and La^+ with alkanes using FT-mass spectrometry and observed dehydrogenated products.[10]

The reactions of group 3 metals with alkanes and the molecular properties of the plausible products have been examined in several theoretical studies. Seigbahn et al. investigated the reactions of the second-row transition metals with methane and the structures of the products, and predicted that yttrium would not be very reactive.[11] A theoretical study of the molecular structures and electronic characteristics of MCH_n (M = K−Mn, $n = 1-3$) by Dobado et al. suggested that the CH_2 group is distorted in $ScCH_2$.[12] The binding energies and structures of carbenes and fluorocarbenes of the first-row transition metals were reported by Dalmázio and Duarte.[13] Finally bonding of the first- and second-row transition metal cations to methylidene ($:CH_2$) was considered theoretically by Bauschlicher et al.[14]

* Author to whom correspondence should be addressed. E-mail: lsa@virginia.edu.

(1) (a) Cho, H.-G.; Andrews, L. *J. Phys. Chem. A* **2004**, *108*, 6294 (Ti + CH_3F). (b) Cho, H.-G.; Andrews, L. *Inorg. Chem.* **2005**, *44*, 979 (Ti + CH_3X). (c) Cho, H.-G.; Andrews, L. *J. Am. Chem. Soc.* **2004**, *126*, 10485 (Zr + CH_3F). (d) Cho, H.-G.; Andrews, L. *Organometallics* **2004**, *23*, 4357 (Hf + CH_3F). (e) Cho, H.-G.; Kim, T.-H.; Andrews, L. *Chem. Asian J.* **2006**, *1*, 404 (Zr, Hf + CH_3X).

(2) (a) Cho, H. G.; Andrews, L. *Organometallics* **2005**, *24*, 477 (Nb + CH_3F). (b) Cho, H.-G.; Andrews, L. *J. Phys. Chem. A* **2006**, *110*, 10063 (V, Nb, and Ta +).

(3) (a) Cho, H.-G.; Andrews, L. *Chem.−Eur. J.* **2005**, *11*, 5017 (Mo + CH_3F). (b) Cho, H.-G.; Andrews, L. *Organometallics* **2005**, *24*, 5678 (Cr, W + CH_3F). (c) Cho, H.-G.; Andrews, L. *J. Phys. Chem. A* **2006**, *110*, ASAP (Mo, W + CH_3X).

(4) (a) Andrews, L.; Cho, H.-G; Wang, X. *Inorg. Chem.* **2005**, *44*, 4834 (Ti + CH_4). (b) Cho, H.-G; Wang, X.; Andrews, L. *Organometallics* **2005**, *24*, 2854 (Hf + CH_4). (c) Andrews, L.; Cho, H.-G.; Wang, X. *Angew. Chem. Int. Ed.* **2005**, *44*, 113 (Zr + CH_4). (d) Cho, H.-G.; Wang, X.; Andrews, L. *J. Am. Chem. Soc.* **2005**, *127*, 465 (Zr+CH_4). Correction for Table 3: the first column is isotopomer 7 with ZPE 18.298, and the sixth column is isotopomer 2 with ZPE 16.930.

(5) Cho, H. G.; Andrews, L. *J. Phys. Chem.* **2006**, *110*, 3886 (V, Nb, and Ta + CH_4).

(6) (a) Cho, H.-G.; Andrews, L. *J. Am. Chem. Soc.* **2005**, *127*, 8226 (Mo + CH_4). (b) Cho, H.-G.; Andrews, L.; Marsden, C. *Inorg. Chem.* **2005**, *44*, 7634 (Cr, W + CH_4).

(7) Andrews, L.; Cho, H.-G. *Organometallics* **2006**, *25*, 4040 (Review article).

(8) (a) Schrock, R. R. *Chem. Rev.* **2002**, *102*, 145. (b) Buchmeiser, M. R. *Chem. Rev.* **2000**, *100*, 1565.

(9) Sunerlin, L. S.; Armentrout, P. B. *J. Am. Chem. Soc.* **1989**, *111*, 3845.

(10) Huang, Y.; Wise, M. B.; Jacobson, D. B.; Freiser, B. S. *Organometallics* **1987**, *6*, 346.

(11) (a) Siegbahn, Per E. M.; Svensson, M. *Chem. Phys. Lett.* **1993**, *216*, 147. (b) Siegbahn, Per E. M.; Blomberg, M. R. A.; Svensson, M. *J. Am. Chem. Soc.* **1993**, *115*, 4191. (c) Blomberg, M. R. A.; Siegbahn, P. E. M.; Svensson, M. *J. Am. Chem. Soc.* **1992**, *114*, 6095.

(12) Vidal, I.; Melchor, S.; Dobado, J. A. *J. Phys. Chem. A* **2005**, *109*, 7500.

(13) Dalmázio, I.; Duarte, H. A. *J. Chem. Phys.* **2001**, *115*, 1747.

(14) Bauschlicher, C. W., Jr.; Partridge, H.; Sheehy, J. A.; Langhoff, S. R.; Rosi, M. *J. Am. Chem. Soc.* **1992**, *96*, 6969.

10.1021/om060816u CCC: $37.00
Publication on Web 12/24/2006

The reactivities of early transition metals with methane and methyl halides show periodic trends. Group 4 metals produce methyl, methylidene, and more stable high-order ($(CH_3)_2MX_2$, X = H, F, Cl, Br) complexes,[1,4] whereas group 6 metals form methyl, methylidene, and methylidyne complexes.[3,6] Group 5 metals, on the other hand, generate methyl, methylidene, anionic methylidyne, and high-order complexes.[2,5] The higher oxidation-state complexes are favored in reaction of second- and third-row transition metals. Late first-row transition metals and Rh give only insertion complexes.[15−18] It is therefore interesting to consider if C−H insertion and following α-hydrogen migration will occur for group 3 metal atom activation of methane and if the products have structures consistent with previously studied early transition metal complexes.[1−7]

In this investigation, reactions of laser-ablated group 3 metal atoms with CH_4 in argon were carried out, and the products isolated in an argon matrix were investigated by means of infrared spectroscopy and supporting quantum chemical calculations. Like other early transition metals, group 3 metals also form methyl hydride and methylidene dihydride complexes in the reaction with methane and upon photolysis afterward, but show a reverse trend in relative yields of these two products. The methylidene dihydride complexes reveal unique structural features with no evidence of agostic distortion.

Experimental and Computational Methods

Laser-ablated group 3 metal atoms (Johnson-Matthey) were reacted with CH_4 (Matheson, UHP grade), $^{13}CH_4$, CD_4, and CH_2D_2 (Cambridge Isotopic Laboratories) in excess argon during condensation at 8 K using a closed-cycle refrigerator (Air Products HC-2). The methods have been described in detail elsewhere.[19,20] Concentrations of gas mixtures are typically 1.0−2.0% in argon. After reaction, infrared spectra were recorded at a resolution of 0.5 cm^{-1} using a Nicolet 550 spectrometer with an MCT-B detector. Samples were later irradiated by a mercury arc lamp (175 W) with a combination of optical filters and were annealed, and more spectra were recorded.

Complementary density functional theory (DFT) calculations were carried out using the Gaussian 03 package,[21] B3LYP density functional,[22] 6-311++G(3df,3pd) basis sets for C, H, and Sc, and SDD pseudopotential and basis set[23] for Y and La to provide a consistent set of vibrational frequencies for the reaction products. More rigorous CCSD calculations[24] were carried out for methylidene products, which often show distinct agostic distortion, and for the methyl hydride products. BPW91[25] and MP2[26] calculations were also done to complement the B3LYP and CCSD results. Geometries were fully relaxed during optimization, and the optimized geometry was confirmed by vibrational analysis. The vibrational frequencies were calculated analytically. In the calculation of binding energy of a metal complex, the zero-point energy is included.

Anharmonic frequency calculations by numerical differentiation[27] (with Gaussian 03 keyword "anharmonic") were also carried out with B3LYP to compare with experimental values and to examine the effects of anharmonicity. While the frequencies are measured in an argon matrix, which typically results in a small 1−2% red shift in the vibrational frequencies from the gas-phase values, the matrix effects were not considered in our calculations.

Results and Discussion

Reactions of Sc, Y, and La with methane isotopomers were done in condensing argon, and the observed product vibrational characteristics and their variations upon photolysis and annealing are compared with the calculated results.

Y + CH_4. The IR spectra from reactions of laser-ablated Y atoms with CH_4, CD_4, and CH_2D_2 are shown in Figures 1−3. Three sets of product absorptions marked **i** (insertion product), **m** (methylidene), and **h** (higher-order product) are observed on the basis of the behaviors upon photolysis and annealing, and the frequencies are listed in Table 1. The Y + CH_4 spectra in the regions 1450−1350, 1130−1080, and 600−450 cm^{-1} are shown in Figure 1, which includes the original spectra after co-deposition with 2.0% CH_4 (a) and 1.0% CH_4 (c) and their variations upon photolysis and annealing (b, d−g). The absorptions marked "**i**" almost triple upon visible ($\lambda > 420$ nm) irradiation (d), while the absorptions marked "**m**" remain virtually unchanged. The **m** absorptions, however, quadruple on UV ($240 < \lambda < 380$ nm) irradiation (e), while the **i** absorptions slightly decrease. In the following process of annealing, the **i** and **m** absorptions sharpen and later decrease (f and g). The absorptions marked with "**h**" increase particularly on annealing (f and g), and they become much stronger at higher concentration of CH_4 (b).

Essentially the same spectral variations upon photolysis and annealing are observed in the Y + CD_4 spectra with 2% (a and b) and 1% (c−g) CD_4, shown in Figure 2. The **i** and **m** absorptions markedly increase upon visible and UV irradiations, respectively, and the **h** absorptions become stronger in the process of annealing and at high concentration. Similar variations are also observed in the Y + CH_2D_2 (2%) spectra, as shown in Figure 3. The **i** and **m** absorptions increase considerably upon visible and UV irradiation, respectively. The **h** absorptions are relatively stronger due to higher concentration.

The strongest new product absorptions are observed in the region 1450−1350 cm^{-1} in Figure 1. The hydrogen stretching

(15) Klabunde, K. J.; Tanaka. Y. *J. Am. Chem. Soc.* **1983**, *105*, 3544.
(16) Klotzbucher, W. E.; Mitchell, S. A.; Ozin, G. A. *Inorg. Chem.* **1977**, *16*, 3063.
(17) (a) Billups, W. E.; Konarski, M. M.; Hauge, R. H.; Margrave, J. L. *J. Am. Chem. Soc.* **1980**, *102*, 7393. (b) Ozin, G. A.; McIntosh, D. F.; Mitchell, S. A.; Garcia-Prieto, J. *J. Am. Chem. Soc.* **1981**, *103*, 1574.
(18) Wang, G.; Chen, M.; Zhou, M. *Chem. Phys. Lett.* **2005**, *412*, 46.
(19) (a) Zhou, M. F.; Andrews, L. *J. Phys. Chem. A* **1998**, *102*, 8251. (b) Wang, X.; Andrews, L. *J. Phys. Chem. A* **2003**, *107*, 570.
(20) Andrews, L.; Citra, A. *Chem. Rev.* **2002**, *102*, 885, and references therein.
(21) Kudin, K. N.; Burant, J. C.; Millam, J. M.; Iyengar, S. S.; Tomasi, J.; Barone, V.; Mennucci, B.; Cossi, M.; Scalmani, G.; Rega, N.; Petersson, G. A.; Nakatsuji, H.; Hada, M.; Ehara, M.; Toyota, K.; Fukuda, R.; Hasegawa, J.; Ishida, M.; Nakajima, T.; Honda, Y.; Kitao, O.; Nakai, H.; Klene, M.; Li, X.; Knox, J. E.; Hratchian, H. P.; Cross, J. B.; Adamo, C.; Jaramillo, J.; Gomperts, R.; Stratmann, R. E.; Yazyev, O.; Austin, A. J.; Cammi, R.; Pomelli, C.; Ochterski, J. W.; Ayala, P. Y.; Morokuma, K.; Voth, G. A.; Salvador, P.; Dannenberg, J. J.; Zakrzewski, V. G.; Dapprich, S.; Daniels, A. D.; Strain, M. C.; Farkas, O.; Malick, D. K.; Rabuck, A. D.; Raghavachari, K.; Foresman, J. B.; Ortiz, J. V.; Cui, Q.; Baboul, A. G.; Clifford, S.; Cioslowski, J.; Stefanov, B. B.; Liu, G.; Liashenko, A.; Piskorz, P.; Komaromi, I.; Martin, R. L.; Fox, D. J.; Keith, T.; Al-Laham, M. A.; Peng, C. Y.; Nanayakkara, A.; Challacombe, M.; Gill, P. M. W.; Johnson, B.; Chen, W.; Wong, M. W.; Gonzalez, C.; Pople, J. A. *Gaussian 03*, Revision B.04; Gaussian, Inc.: Pittsburgh, PA, 2003.
(22) (a) Becke, A. D. *J. Chem. Phys.* **1993**, *98*, 5648. (b) Lee, C.; Yang, Y.; Parr, R. G. *Phys. Rev. B* **1988**, *37*, 785.
(23) Andrae, D.; Haeussermann, U.; Dolg, M.; Stoll, H.; Preuss, H. *Theor. Chim. Acta* **1990**, *77*, 123.
(24) Pople, J. A.; Krishnan, R.; Schlegel, H. B.; Binkley, J. S. *Int. J. Quantum Chem.* **1978**, *14*, 545.
(25) Burke, K.; Perdew, J. P.; Wang, Y. In *Electronic Density Functional Theory*: *Recent Progress and New Directions*; Dobson, J. F., Vignale, G., Das, M. P., Ed.; Plenum: New York, 1998.
(26) Frisch, M. J.; Head-Gordon, M.; Pople, J. A. *Chem. Phys. Lett.* **1990**, *166*, 281.
(27) Page, M.; Doubleday, C.; McIver, J. W., Jr. *J. Chem. Phys.* **1990**, *93*, 5634.

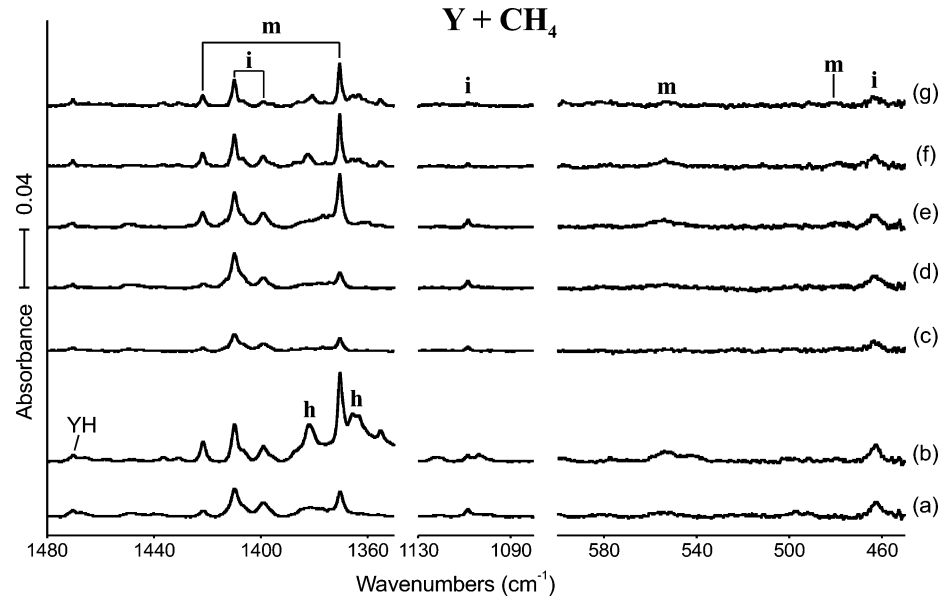

Figure 1. IR spectra in the regions 1450−1350 and 1130−1080 cm^{-1} for laser-ablated Y atoms co-deposited with CH_4 in excess argon at 8 K and their variation. (a) Y + 2.0% CH_4 in Ar co-deposited for 1 h. (b) Y + 2.0% CH_4 after broadband photolyses with $\lambda > 420$ nm and $240 < \lambda < 380$ nm and annealing to 36 K in sequence. (c) Y + 1.0% CH_4 in Ar co-deposited for 1 h. (d) After broadband photolysis with a filter ($\lambda > 420$ nm) for 20 min. (e) After broadband photolysis with a filter ($240 < \lambda < 380$ nm) for 20 min. (f) After annealing to 28 K. (g) After annealing to 44 K. **i**, **m**, and **h** denote the product absorption groups.

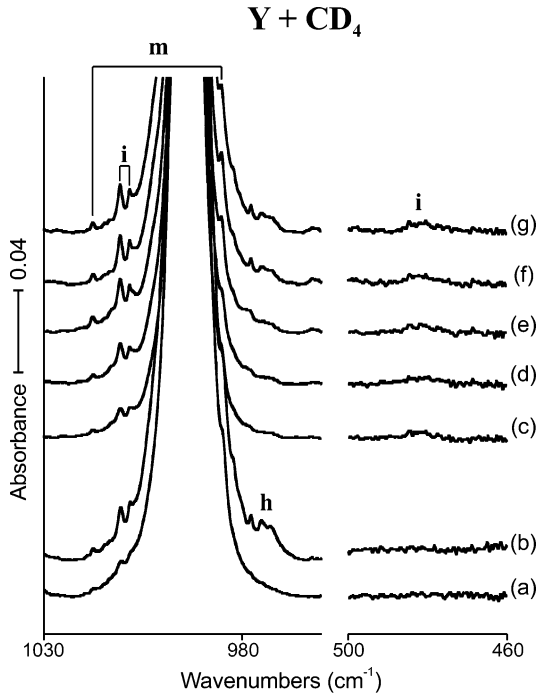

Figure 2. IR spectra in the regions 1030−960 and 500−460 cm^{-1} for laser-ablated Y atoms co-deposited with CD_4 in excess argon at 8 K and their variation. (a) Y + 2.0% CD_4 in Ar co-deposited for 1 h. (b) Y + 2.0% CD_4 after broadband photolyses with $\lambda > 420$ nm and $240 < \lambda < 380$ nm and annealing to 36 K in sequence. (c) Y + 1.0% CD_4 in Ar co-deposited for 1 h. (d) After broadband photolysis with a filter ($\lambda > 420$ nm) for 20 min. (e) After broadband photolysis with a filter ($240 < \lambda < 380$ nm) for 20 min. (f) After annealing to 28 K. (g) After annealing to 36 K. **i**, **m**, and **h** denote the product absorption groups, and the strong band at 993 cm^{-1} is due to CD_4.

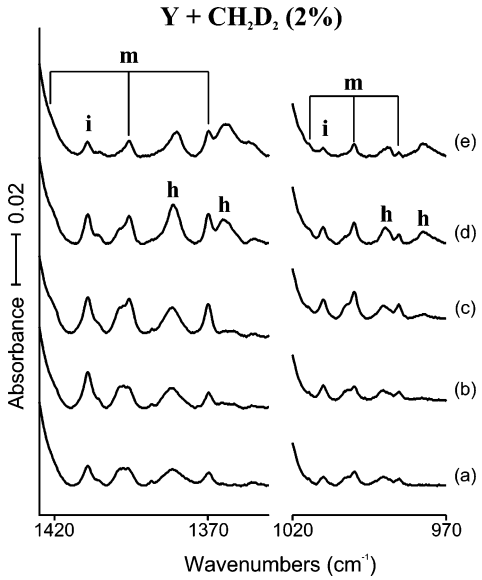

Figure 3. IR spectra in the regions 1425−1350 and 1020−970 cm^{-1} for laser-ablated Y atoms co-deposited with CH_2D_2 in excess argon at 8 K and their variation. (a) Y + 2.0% CH_2D_2 in Ar co-deposited for 1 h. (b) After broadband photolysis with a filter ($\lambda > 420$ nm) for 20 min. (c) After broadband photolysis with a filter ($240 < \lambda < 380$ nm) for 20 min. (d) After annealing to 28 K. (e) After annealing to 28 K. **i**, **m**, and **h** denote the product absorption groups.

absorptions of binary yttrium hydrides have been observed previously in this region from hydrogen reactions, and it was also reported that higher oxidation-state group 3 metal hydrides give relatively lower M−H stretching frequencies.[28] In the present study weak YH, YH_4^-, YD, and YD_4^- absorptions are also observed at 1470.3, 1227.3, 1052.9, and 882.3 cm^{-1}, respectively.

The strong **i** absorption at 1409.7 cm^{-1} has its deuterium counterpart at 1010.8 cm^{-1} (H/D ratio of 1.395) but shows essentially no ^{13}C shift, indicating that it is a Y−H stretching absorption of a primary product. This single, strong Y−H

(28) (a) Wang, X.; Chertihin, G. V.; Andrews, L. *J. Phys. Chem. A* **2002**, *106*, 9213. (b) Wang, X.; Andrews, L. *J. Am. Chem. Soc.* **2002**, *124*, 7610.

Table 1. Frequencies of Product Absorptions Observed from Reactions of Methane with Y in Excess Argon[a]

	CH_4	CD_4	$^{13}CH_4$	CH_2D_2	description
i	**1409.7**, 1399.0	**1010.8**, 1008.4	**1409.4**, 1398.4	1409.4, 1010.1	Y−H str.
	1108.6, 1103.9	870.2	**1099.5**, 1095.1		CH_3 deform
	462.4		455.9		C−Y str.
m	1421.6	1017.8	1421.3	1421 sh, **1395.8**, 1369.9	YH_2 str.
	1370.3	985.5	1370.1	1016.8, **1000.0**, 985.5	YH_2 str.
	554.5	481.7	550.8		YH_2 scis.
	479.6		476.9		CH_2 wag
h	1382.1		1381.5	1381.5, 990.5	Y-H str.
	1363.1	975.2	1364.5	1363.0, 977.3	Y-H str.

[a] All frequencies are in cm^{-1}. Stronger absorptions in a set are bold. Description gives major coordinate. **i**, **m**, and **h** stand for insertion, methylidene, and higher-order products, respectively.

Table 2. Calculated Fundamental Frequencies of CH_3-YH Isotopomers in the Ground $^2A'$ Electronic State[a]

	CH_3-YH				CD_3-YD			$^{13}CH_3-YH$		
approximate description	B3LYP (anharm)[b]	B3LYP	BPW91	int.	B3LYP	BPW91	int.	B3LYP	BPW91	int.
A′ CH_3 str.	2882.1	3045.2	2999.0	12	2249.9	2216.1	5	3034.7	2988.6	12
A′ CH_3 str.	2828.7	2964.4	2914.8	10	2125.5	2089.0	2	2961.4	2912.0	10
A′ Y−H str.	1418.7	1454.3	1384.4	405	1034.9	1003.4	188	1454.3	1382.3	405
A′ CH_3 bend	1406.0	1420.5	1377.4	5	1030.0	981.1	21	1416.8	1376.4	5
A′ CH_3 deform	1106.5	1139.0	1085.4	18	888.7	844.2	29	1130.2	1077.2	16
A′ C−Y str.	464.3	470.1	451.8	99	408.2	391.1	57	463.9	446.8	96
A′ CYH bend	392.9	420.1	413.0	9	332.0	327.2	11	412.3	404.7	10
A′ CH_3 rock	282.9	265.0	260.4	37	188.8	186.4	20	264.8	260.0	37
A″ CH_3 str.	2864.9	3030.9	2990.9	9	2238.9	2208.2	3	3020.4	2980.8	9
A″ CH_3 bend	1374.9	1427.0	1377.2	9	1035.8	999.8	6	1423.7	1374.0	9
A″ CH_2 rock	321.1	342.8	267.1	2	255.7	189.4	2	341.1	266.9	2
A″ CH_3 distort	90.9	92.2	121.5	37	65.5	85.8	19	92.2	121.5	37

[a] Frequencies and intensities computed with 6-311++G(3df, 3pd) are for harmonic calculations except where otherwise noted. The SDD core potential and basis set are used for Y. Intensities are calculated with B3LYP. Frequencies and intensities are in cm^{-1} and km/mol. [b] Calculated anharmonic frequencies.

Table 3. Calculated Fundamental Frequencies of Yttrium Methylidene Hydride (CH_2-YH_2) Isotopomers in the Ground $^2B_1$ Electronic State[a]

	CH_2-YH_2					CD_2-YD_2			$^{13}CH_2-YH2$			CHD−YHD		
approximate description	B3LYP (anharm)[b]	B3LYP	MP2	CCSD	int.	B3LYP	CCSD	int.	B3LYP	CCSD	int.	B3LYP	CCSD	int.
A_1 CH_2 str.	2883.4	3019.2	3088.0	3044.0	20	2190.3	2210.0	4	3013.4	3038.0	22	2236.5	2254.3	5
A_1 YH_2 str.	1436.5	1467.5	1515.9	1491.8	336	1041.5	1058.4	184	1467.5	1491.8	336	1027.9	1040.8	350
A_1 CH_2 scis.	1357.2	1371.1	1390.9	1397.4	0	1020.8	1040.1	0	1362.6	1391.7	1	1211.9	1233.9	2
A_1 YH_2 scis.	564.6	590.3	593.3	584.5	349	478.8	489.6	176	586.1	580.6	343	538.6	542.4	274
A_1 C−Y str.	462.0	469.0	469.9	466.6	0	375.4	370.7	38	457.8	456.1	1	443.1	438.7	10
A_2 CH_2 twist	215.2	180.3	173.6	177.8	0	127.7	125.7	0	180.3	177.8	0	216.6	144.5	6
B_1 CH_2 wag	553.1	567.8	519.5	517.7	92	455.4	404.8	70	564.1	513.3	89	519.2	466.6	82
B_1 YH_2 wag	69.4	176.4	105.5	120.9	708	127.4	87.5	368	176.3	120.8	708	155.8	104.2	513
B_2 CH_2 str.	2930.2	3087.1	3164.7	3110.4	22	2285.2	2301.0	8	3075.8	3099.2	22	3054.4	3078.3	21
B_2 YH_2 str.	1389.1	1421.3	1460.3	1433.8	873	1014.6	1024.3	453	1421.3	1433.8	873	1444.6	1462.3	574
B_2 CH_2 rock	425.3	453.7	426.0	422.3	60	350.2	327.1	33	450.5	419.2	60	380.0	352.5	43
B_2 YH_2 rock	234.1	261.3	182.6	177.1	9	185.7	126.1	5	261.2	177.0	9	148.6	149.0	24

[a] Frequencies and intensities computed with 6-311++G(3df, 3pd) are for harmonic calculations except where otherwise noted. The SDD core potential and basis set are used for Y. Intensities are calculated with CCSD/6-311++G(3df,3pd)/SDD. Frequencies and intensities are in cm^{-1} and km/mol. CH_2-YH_2 has a C_s structure with B3LYP and BPW91, whereas it has a C_{2v} structure at the levels of MP2 and CCSD. The symmetry notations are based on the C_{2v} structure. [b] Calculated anharmonic frequencies.

stretching band with a relatively high frequency shows that C−H insertion by yttrium readily occurs in reaction with CH_4 and upon visible photolysis afterward to form the primary product, CH_3-YH, which will be identified from comparison of the three observed frequencies with calculated values (Table 2) for these three strongest infrared absorptions using DFT.[29]

A much weaker **i** absorption is observed at 1108.6 cm^{-1}, and its D and ^{13}C counterparts are observed at 870.2 (not shown) and 1099.5 cm^{-1} (H/D and $^{12}C/^{13}C$ ratios of 1.274 and 1.008), respectively. On the basis of the observed frequencies, and the large H/D and small $^{12}C/^{13}C$ ratios, the **i** absorptions are attributed to the CH_3 deformation mode. The calculated (8.8 cm^{-1}) and observed (9.1 cm^{-1}) carbon-13 shifts are in good agreement. On the further low-frequency side, another **i** absorption with observable intensity is located at 462.4 cm^{-1} and its ^{13}C counterpart at 455.9 cm^{-1} (shift 6.5 cm^{-1}). The deuterium counterpart is calculated to be below our instrumental limit. The band is assigned to the C−Y stretching mode, which is coupled with the CYH bending mode, and has a calculated 6.2 cm^{-1} carbon-13 shift. The observed vibrational characteristics substantiate formation of the C−H insertion complex (CH_3-YH).

The two strong, associated absorptions at 1421.6 and 1370.3 cm^{-1} with 1:2 intensity ratio show D shifts of −403.8 and −384.8 cm^{-1} (H/D isotopic ratios of 1.397 and 1.390) but very small ^{13}C shifts, indicating that a second product with two Y−H

(29) (a) Scott, A. P.; Radom, L. *J. Phys. Chem.* **1996**, *100*, 16502. (b) Andersson, M. P.; Uvdal, P. L. *J. Phys. Chem. A* **2005**, *109*, 3937.

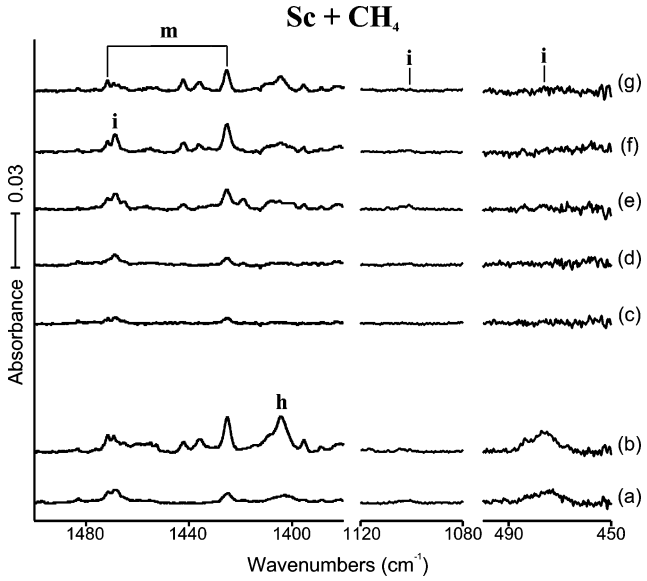

Figure 4. IR spectra in the regions 1500−1380, 1120−1080, and 500−450 cm^{-1} for laser-ablated Sc atoms co-deposited with CH_4 in excess argon at 8 K and their variation. (a) Sc + 2.0% CH_4 in Ar co-deposited for 1 h. (b) Sc + 2.0% CH_4 after broadband photolyses with $\lambda > 420$ nm and $240 < \lambda < 380$ nm and annealing to 36 K in sequence. (c) Sc + 1.0% CH_4 in Ar co-deposited for 1 h. (d) After broadband photolysis with a filter ($\lambda > 420$ nm) for 20 min. (e) After broadband photolysis with a filter ($240 < \lambda < 380$ nm) for 20 min. (f) After annealing to 28 K. (g) After annealing to 42 K. **i**, **m**, and **h** denote the product absorption groups.

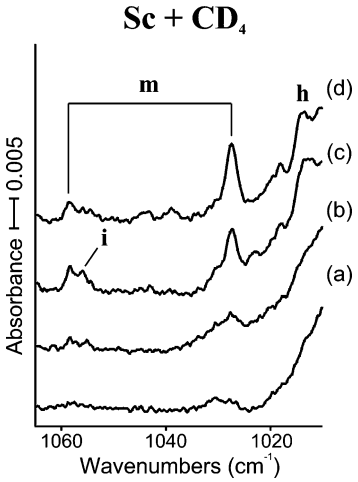

Figure 5. IR spectrum in the region 1650−1010 cm^{-1} for laser-ablated Sc atoms co-deposited with CD_4 in excess argon at 8 K and their variation. (a) Sc + 2.0% CD_4 in Ar co-deposited for 1 h. (b) After broadband photolysis with a filter ($\lambda > 420$ nm) for 20 min. (c) After broadband photolysis with a filter ($240 < \lambda < 380$ nm) for 20 min. (d) After annealing to 28 K. **i**, **m**, and **h** denote the product absorption groups.

Table 4. Frequencies of Product Absorptions Observed from Reactions of Methane with Sc in Excess Argon[a]

	CH_4	CD_4	$^{13}CH_4$	CH_2D_2	description
i	1469.0	1055.9	1468.8	1468.1	Sc−H str.
	1100.9		1092.4		CH_3 deform
	475.4		467.8	460.1	C−Sc str.
m	1471.6	1058.4	1471.5	1059.7	ScH_4 str.
	1425.0	1027.5	1424.7		ScH_4 str.
h	1405.2	1013.4	1405.3	1402.9, 1009.9	Sc−H str.

[a] All frequencies are in cm^{-1}. Description gives major coordinate. **i**, **m**, and **h** stand for insertion, methylidene, and higher-order products, respectively.

bonds is formed in the reaction of Y with CH_4 and particularly on UV photolysis afterward. The most probable product with two Y−H bonds is the methylidene dihydride complex, CH_2−YH_2, based on the observation of α-H transfer in previous work with group 4−6 complexes,[4−7] and calculated frequencies are listed in Table 3.

The excess energy resulting from the C−H insertion reaction by the metal atom either dissipates into the cold matrix or initiates the following α-hydrogen migration to form the methylidene complex.[1−7] The **m** absorptions are originally relatively weak in the hydrogen stretching frequency region and remain weak upon visible irradiation; however, they increase more than the **i** absorption upon UV irradiation.

In the low-frequency region, a weak **m** absorption is observed at 554.5 cm^{-1}, and its D and ^{13}C counterparts are observed at 481.7 and 550.8 cm^{-1} (H/D and $^{12}C/^{13}C$ ratios of 1.151 and 1.007). They are attributed to the YH_2 scissoring mode, which is coupled with the C−Y stretching mode. On the further low-frequency side, another absorption at 479.6 m^{-1} is observed with the ^{13}C counterpart at 476.9 cm^{-1} (shift 2.7 cm^{-1}). The deuterium counterpart is not observed, probably due to its low frequency. These bands are assigned to the CH_2 wagging mode.

The observed CH_2 wagging frequency is considerably lower than those of group 4−6 metal methylidenes,[1−6] suggesting that the carbon−metal bond is not as rigid. The Y methylidene complex apparently has two equal Y−H bonds, on the basis of the Y−H stretching frequency absorption of CHD−YHD at the middle of the YH_2 stretching absorption pair for CH_2−YH_2 and the Y−D band likewise between those for the YD_2 pair for CD_2−YD_2, shown in Figure 3 and Table 1. The computation results also support that the product has two equivalent C−H and two equivalent Y−H bonds, while yielding different structures at the metal center. The CH_2−YH_2 structure has C_s symmetry with two equal slightly out-of-plane Y−H bonds using B3LYP and BPW91 with 6-311++G(3df,3pd), whereas it has a C_{2v} structure with the MP2 and CCSD methods. The symmetric structure is in fact surprising because most previously studied methylidene hydride complexes of early transition metals have considerably distorted structures owing to agostic interaction.[4−6]

The CH_2D_2 experiment also reveals two absorptions for CH_2−YD_2 (1016.8 and 985.5 cm^{-1}) and two Y−H stretching bands for CD_2−YH_2 (1421 cm^{-1} shoulder on precursor and 1369.9 cm^{-1}). The presence of these absorptions along with stronger Y−H and Y−D stretching absorptions for CHD−YHD indicates that both H and D transfer occur in these complexes, but the CD_2−YH_2 product is favored over the CH_2−YD_2 product [the 1369.9 cm^{-1} band is 4 times stronger than the 985.5 cm^{-1} band, and the calculated relative intensities for these modes is 2:1]. We expect H transfer to be faster, and we have observed a kinetic isotope effect on the yield of CH_2═VHF relative to CD_2═VDF in V experiments with methyl fluoride.[2b] We also notice that electronic energy with zero-point vibrational energy (ZPE) correction included places CD_2−YH_2 1.6 kcal/mol lower in energy than CH_2−YD_2. The CHD−YHD isotopic modification has double statistical weight (cis and trans have virtually the same ZPE and frequencies) and is 0.8 kcal/mol higher in energy than CD_2−YH_2. A similar preference was found for the more stable CD_2═ZrH_2 isotopic modification over CH_2═ZrD_2 in recent Zr reactions with CH_2D_2.[4d]

Owing to the detection of YH_4^- in this and previous laser ablation experiments,[28] we have calculated the stable anion CH_2═YH_2^- to help locate this species and to compare with the agostic isoelectronic methylidene CH_2═ZrH_2 complex inves-

Table 5. Calculated Fundamental Frequencies of CH_3-ScH Isotopomers in the Ground $^2A'$ Electronic State[a]

	CH_3-Sc-H				CD_3-ScD			$^{13}CH_3-ScH$		
approximate description	B3LYP (anharm)[b]	B3LYP	BPW91	int.	B3LYP	BPW91	int.	B3LYP	BPW91	int.
A′ CH_3 str.	2893.8	3053.5	3014.0	10	2256.7	2227.7	4	3042.9	3003.5	10
A′ CH_3 str.	2836.1	2971.7	2921.9	7	2129.6	2093.5	1	2968.8	2919.1	6
A′ Sc−H str.	1456.0	1516.3	1515.8	532	1084.7	1084.2	277	1516.3	1515.8	532
A′ CH_3 bend	1399.2	1418.1	1367.1	2	1029.3	992.3	1	1414.9	1364.0	1
A′ CH_3 deform	1101.5	1134.3	1085.2	11	890.6	855.7	28	1125.0	1076.0	9
A′ C−Sc str.	489.2	512.6	510.6	143	452.3	453.2	91	505.5	502.9	140
A′ CScH bend	401.2	446.2	451.3	4	350.2	350.2	7	440.0	445.8	5
A′ CH_3 rock	270.5	279.3	274.1	41	199.8	196.4	22	279.0	273.8	40
A″ CH_3 str.	2876.3	3043.3	3005.3	10	2248.8	2221.1	3	3032.8	2994.9	10
A″ CH_3 bend	1378.2	1425.4	1376.1	8	1034.4	998.8	6	1422.1	1372.9	7
A″ CH_2 rock	337.4	361.2	342.8	9	270.7	256.7	7	359.4	341.1	8
A″ CH_3 distort	44.3	100.4	85.1	63	71.7	60.5	33	100.4	85.1	63

[a] Frequencies and intensities computed with 6-311++G(3df, 3pd) are for harmonic calculations except where otherwise noted. The all-electron basis is used for Sc. Frequencies and intensities are in cm^{-1} and km/mol. Intensities are calculated with B3LYP. [b] Calculated anharmonic frequencies.

Table 6. Calculated Fundamental Frequencies of Scandium Methylidene Hydride (CH_2-ScH_2) Isotopomers in the Ground $^2B_1$ Electronic State[a]

	CH_2-ScH_2					CD_2-ScD_2			$^{13}CH_2-ScH_2$			CHD−ScHD		
approximate description	B3LYP (anharm)[b]	B3LYP	BPW91	CCSD	int.	B3LYP	CCSD	int.	B3LYP	CCSD	int.	B3LYP	CCSD	int.
A_1 CH_2 str.	2899.6	3031.5	2970.1	3059.2	9	2199.1	2220.9	1	3025.7	3053.2	10	2247.2	2267.5	3
A_1 ScH_2 str.	1511.9	1572.1	1530.1	1620.0	334	1117.7	1151.7	186	1572.1	1620.0	334	1104.8	1135.0	332
A_1 CH_2 scis.	1353.4	1362.8	1315.4	1399.0	0	1019.2	1044.8	7	1357.0	1393.1	0	1206.1	1237.1	4
A_1 ScH_2 scis.	619.9	647.0	643.1	641.1	320	550.8	556.0	173	642.7	635.4	317	604.6	603.4	250
A_1 C−Sc str.	506.2	509.6	506.1	503.0	2	401.2	388.9	31	499.9	494.6	1	478.3	467.9	16
A_2 CH_2 twist	207.8	189.9	187.0	153.0	0	134.3	108.2	0	189.9	153.0	0	160.1	126.6	2
B_1 CH_2 wag	576.1	598.2	563.4	627.7	89	469.3	492.7	69	593.0	622.2	86	539.3	565.3	80
B_1 ScH_2 wag	137.2	121.5	110.4	231.7	589	89.5	170.5	313	121.5	231.6	589	104.9	204.2	448
B_2 CH_2 str.	2951.8	3104.0	3049.8	3131.1	15	2298.5	2317.2	5	3092.6	3119.7	15	3069.3	3096.6	12
B_2 ScH_2 str.	1452.4	1515.6	1483.5	1552.7	790	1092.1	1119.0	421	1515.6	1552.7	790	1544.2	1587.0	535
B_2 CH_2 rock	449.2	472.0	469.2	455.0	49	369.1	355.7	27	468.5	451.6	49	397.3	383.5	35
B_2 ScH_2 rock	248.8	255.9	245.8	240.0	9	182.6	171.3	5	255.9	239.9	9	208.1	195.3	6

[a] Frequencies and intensities computed with 6-311++G(3df, 3pd) are for harmonic calculations except where otherwise noted. The all-electron basis is used for Sc, but in CCSD calculation the SDD core potential and basis set are used instead. Intensities are calculated with CCSD. Frequencies and intensities are in cm^{-1} and km/mol. CH_2-ScH_2 has a C_{2v} structure at all levels of calculation performed in this study. [b] Calculated anharmonic frequencies.

tigated earlier.[4d] The strong Y−H stretching frequencies are computed at 1169 and 1228 cm^{-1}, and unfortunately these are not found in the present experiments. The distorted C_s (planar) structure computed for $CH_2{=}YH_2^-$ is nearly the same as that calculated for the zirconium methylidene dihydride complex, although the latter is pyramidal at the zirconium center. However, the agnostic H′−C−Y angle (92.6°) is almost the same, but the C═Y bond (2.141 Å) is longer.

The **h** absorptions increase gradually in the process of photolysis, but become much stronger on annealing and at higher methane concentration. This evidence suggests that the **h** absorptions arise from the high-order methane complexes. Figure 1 also shows that the band at 1382.1 cm^{-1} increases first and decreases later in annealing, whereas the other band at 1363.1 cm^{-1} increases in the last stage of annealing, indicating that it arises from an even higher-order complex. No attempt has been made to determine the structures of these complexes. The addition of an H atom to the above methyl hydride or methylidene complexes would form CH_3-YH_2, which is a stable dihydride, analogous to the $(CH_3)_2ZrH_2$ molecule prepared previously.[4d] However, the strong diagnostic absorptions for CH_3-YH_2 are computed to be 11 and 7 cm^{-1} above those for CH_2-YH_2, respectively, and to have 5:3 relative intensities. Although the **h** band at 1382 cm^{-1} is a possibility, there is no absorption of appropriate intensity in the 1430−1440 cm^{-1} region for this species. Hence, we have produced insufficient H atoms to also form CH_3-YH_2 in these experiments.

Sc + CH_4. The IR spectra from reactions of laser-ablated Sc atoms with CH_4 and CD_4 are shown in Figures 4 and 5, where the spectral features and their variations are similar to those in the Y spectra. The CH_2D_2 spectra, where many important features are covered by precursor absorptions, are not shown here. Parallel to the case of Y + CH_4, three sets of product absorptions marked "**i**, **m**, and **h**" are observed on the basis of the behaviors upon photolysis and annealing, and the frequencies are listed in Table 4. The **i** absorptions are relatively weaker in comparison with the Y case. Both the **i** and **m** absorptions are discernible in the original spectra after deposition. The **i** absorptions double upon visible irradiation (d) and increase another 100% upon UV irradiation (e) (triple in total). The **m** absorptions increase about 30% and quadruple upon visible and UV irradiations (d and e), respectively. While both the **i** and **m** absorptions sharpen and later decrease in the process of annealing (f and g), the **h** absorptions increase. The product responsible for the **i** absorptions appears to be less stable on annealing (g). Weak binary scandium hydride absorptions were also observed at 1530.4, 1360.9, and 1103.4 cm^{-1} originating from ScH, $H_2Sc(H_2)$, and ScD, repectively.[28]

The **i** absorption at 1469.0 cm^{-1} has its deuterium counterpart at 1055.9 cm^{-1} (H/D ratio of 1.391) but shows essentially no ^{13}C shift. The frequencies are compared with the hydrogen stretching frequencies of ScH_3, $(H_2)ScH_2$, and ScD_3 at 1487.8, 1414.1, and 1079.1 cm^{-1}, respectively.[28] Parallel to the Y case, the single **i** absorption in the Sc−H stretching absorption region is assigned to the Sc−H stretching mode of the C−H insertion product, CH_3-ScH. A weak absorption at 1100.9 cm^{-1} has its ^{13}C counterpart at 1092.4 cm^{-1} (not shown) ($^{12}C/^{13}C$ ratio of 1.008), but the deuterium counterpart is not observed. The band

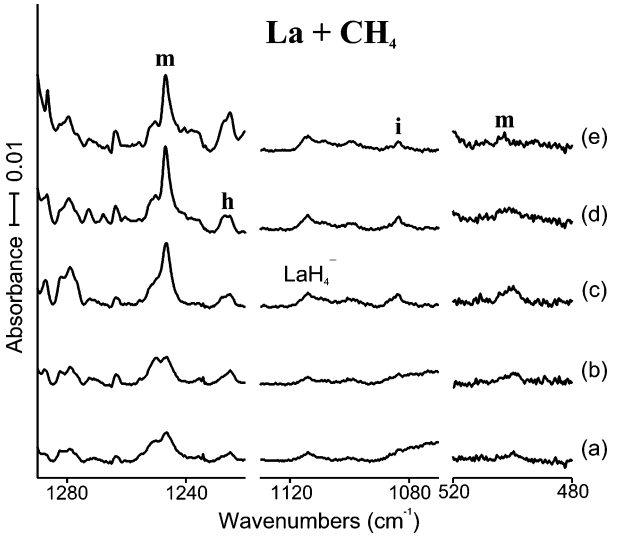

Figure 6. IR spectra in the regions 1290−1220, 1130−1070, and 520−480 cm^{-1} for laser-ablated La atoms co-deposited with CH_4 in excess argon at 8 K and their variation. (a) La + 1.0% CH_4 in Ar co-deposited for 1 h. (b) After broadband photolysis with a filter (λ > 420 nm) for 20 min. (c) After broadband photolysis with a filter (240 < λ < 380 nm) for 20 min. (d) After annealing to 28 K. After broadband photolysis with a filter (λ > 220 nm) for 10 min (e) After annealing to 36 K. **i**, **m**, and **h** denote the product absorption groups.

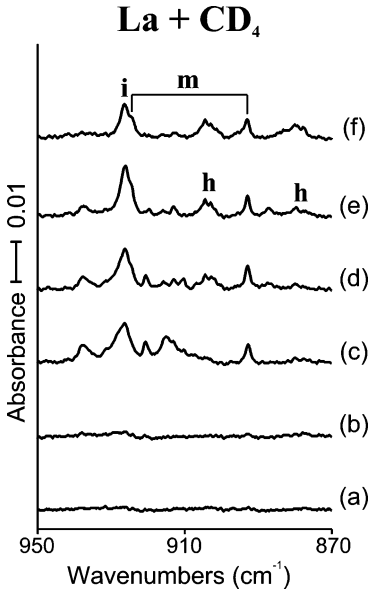

Figure 7. IR spectrum in the region 950−870 cm^{-1} for laser-ablated La atoms co-deposited with CD_4 in excess argon at 8 K and their variation. (a) La + 1.0% CD_4 in Ar co-deposited for 1 h. (b) After broadband photolysis with a filter (λ > 420 nm) for 20 min. (c) After broadband photolysis with a filter (240 < λ < 380 nm) for 20 min. (d) After annealing to 28 K. (e) After annealing to 36 K. (f) After annealing to 44 K. **i**, **m**, and **h** denote the product absorption groups.

is attributed to the CH_3 deformation mode. Another weak absorption at 475.4 cm^{-1} in the further low-frequency region has its ^{13}C counterpart at 467.8 cm^{-1} (not shown) ($^{12}C/^{13}C$ ratio of 1.016). The absorption is assigned to the C−Sc stretching mode on the basis of the frequency and relatively large ^{13}C shift. Therefore, the observed **i** absorptions in the low-frequency region also corroborate formation of the C−H insertion product (CH_3−ScH) in the reaction of Sc with CH_4 and photolysis afterward.

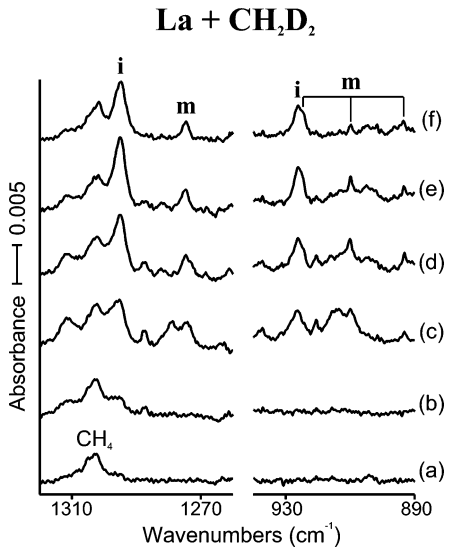

Figure 8. IR spectra in the regions 1320−1260 and 940−890 cm^{-1} for laser-ablated La atoms co-deposited with CH_2D_2 in excess argon at 8 K and their variation. (a) Ta + 1.0% CH_2D_2 in Ar co-deposited for 1 h. (b) After broadband photolysis with a filter (λ > 420 nm) for 20 min. (c) After broadband photolysis with a filter (240 < λ < 380 nm) for 20 min. (d) After annealing to 28 K. (e) After annealing to 36 K. (f) After annealing to 44 K. **i**, **m**, and **h** denote the product absorption groups.

Table 7. Frequencies of Product Absorptions Observed from Reactions of Methane with La in Excess Argon[a]

	CH_4	CD_4	$^{13}CH_4$	CH_2D_2	description
i	*b*	926.3	*b*	1294.8, 925.9	La−H str.
	1083.5	825.2	1074.2		CH_3 deform
m	*b*	924.5	*b*	1274	LaH_2 str.
	1246.8	892.9	1246.8	924.5, **909.9**, 893.2	LaH_2 str.
	499.7		491.9		CH_2 wag
h	1225.2	904.5, 879.8	1225.7		La−H str.

[a] All frequencies are in cm^{-1}. Stronger absorptions are bold. Description gives major coordinate. [b] Overlapped by precursor absorption.

While the **m** absorptions at 1471.6 and 1425.0 cm^{-1} show negligible ^{13}C shifts, as shown in Table 4, they yield large D shifts of −413.2 and −397.5 cm^{-1} (H/D isotopic frequency ratios of 1.390 and 1.387). The **m** absorptions with about 1:2 intensity ratio suggest formation of another primary product with two Sc−H bonds (CH_2−ScH_2) in the reaction of Sc with CH_4 and photolysis afterward. Formation of CH_3−ScH by initial C−H insertion of CH_4 by Sc is evidently followed by α-hydrogen migration, which leads to the methylidene complex (CH_2−ScH_2), and the methylidene complex appears to be relatively more stable in the process of annealing than the insertion complex, as shown in Figure 4. This is compared with the Y case, where the insertion complex persists along with the methylidene product until the last stage of annealing.

The calculated frequencies for CH_3−ScH and CH_2−ScH_2 reproduce the experimental values within the limits of the approximations involved (Tables 5 and 6).[29] Particularly the anharmonic frequencies (B3LYP) are in very good agreement with the experimental values within 3% at most. Structure calculations also show that the smallest possible Sc methylidene dehydride is not agostic, which is consistent with the case of CH_2−YH_2. A C_{2v} structure is predicted for CH_2−ScH_2 at all levels of calculational theory carried out in this study

Similar to the Y case, the **h** absorptions are attributed to a higher-order methane complex.

La + CH_4. Shown in Figures 6−8 are the IR spectra from reactions of laser-ablated La atoms with CH_4 and CD_4, and

Table 8. Calculated Fundamental Frequencies of CH_3-LaH Isotopomers in the Ground $^2A'$ Electronic State[a]

	CH_3-La-H				CD_3-LaD			$^{13}CH_3-LaH$		
approximate description	B3LYP (anharm)[b]	B3LYP	BPW91	int.	B3LYP	BPW91	int.	B3LYP	BPW91	int.
A′ CH_3 str.	2868.8	3044.0	3000.8	14	2249.2	2217.4	5	3033.5	2990.5	14
A′ CH_3 str.	2822.6	2954.6	2903.0	10	2117.7	2080.5	2	2951.6	2900.1	10
A′ CH_3 bend	1378.7	1413.9	1365.4	1	1026.8	991.5	2	1410.7	1362.2	1
A′ La−H str.	1314.0	1335.2	1293.9	674	947.9	918.6	339	1335.2	1293.9	674
A′ CH_3 deform	1096.0	1127.3	1081.4	17	880.5	846.8	35	1118.3	1071.5	14
A′ C−La str.	390.9	420.1	412.6	139	365.6	362.7	82	413.7	404.8	134
A′ CLaH bend	353.6	377.5	369.2	10	295.3	285.4	15	370.7	363.9	12
A′ CH_3 rock	402.5	221.2	202.9	57	157.2	144.1	30	221.1	202.9	57
A′ CH_3 str.	2865.9	3023.3	2981.7	16	2234.0	2203.3	6	3012.8	2971.3	16
A″ CH_3 bend	1354.8	1423.1	1374.8	8	1033.6	998.5	5	1419.8	1371.6	8
A″ CH_2 rock	283.1	292.1	274.0	2	217.3	203.8	2	290.7	272.7	2
A″ CH_3 distort	3.1	99.9	89.0	44	70.7	62.9	23	99.9	89.0	44

[a] Frequencies and intensities computed with 6-311++G(3df, 3pd) are for harmonic calculations except where otherwise noted, and the SDD core potential and basis set are used for La. Intensities are calculated with B3LYP. Frequencies and intensities are in cm^{-1} and km/mol. [b] Calculated anharmonic frequencies.

Table 9. Calculated Fundamental Frequencies of Lanthanum Methylidene Hydride (CH_2-LaH_2) Isotopomers in the Ground $^2A'$ Electronic State[a]

	CH_2-LaH_2				CD_2-LaD_2			$^{13}CH_2-LaH_2$			CHD−LaHD		
approximate description	B3LYP (anharm)[b]	B3LYP	BPW91	int.	B3LYP	BPW91	int.	B3LYP	BPW91	int.	B3LYP	BPW91	int.
A′ CH_2 str.	2859.8	3001.9	2940.1	26	2176.9	2132.0	6	2996.2	2934.6	28	2224.7	2181.2	7
A′ LaH_2 str.	1218.7	1377.7	1350.6	418	975.0	956.7	245	1377.4	1350.6	434	954.0	939.0	435
A′ CH_2 scis.	1319.6	1355.5	1310.8	73	1011.9	978.3	5	1350.2	1305.4	58	1199.7	1159.2	0
A′ CH_2 wag	501.1	535.2	517.0	62	418.9	409.6	62	530.8	513.5	60	482.3	466.5	63
A′ LaH_2 scis.	451.2	488.6	478.0	277	412.9	399.6	143	486.9	476.1	264	451.0	439.2	241
A′ C-La str.	409.4	431.4	430.8	83	337.9	337.2	66	419.9	418.8	91	406.0	406.5	47
A′ LaH_2 scis.	57.7	250.5	233.0	334	179.9	167.4	171	250.3	232.8	332	225.9	209.6	205.9
A″ CH_2 str.	2909.0	3073.4	3017.4	22	2275.4	2233.8	8	3062.1	3006.4	22	3039.1	2980.5	24
A″ LaH_2 str.	1131.4	1315.7	1298.2	1077	935.5	923.1	550	1315.7	1298.2	1077	1346.9	1324.9	749
A″ CH_2 rock	388.3	400.8	394.0	22	307.1	302.3	14	398.1	391.2	22	339.3	333.0	29
A″ LaH_2 rock	219.2	233.1	219.4	0	165.6	155.8	0	233.0	219.3	0	181.5	171.6	42
A″ CH_2 wist	160.7	133.7	107.6	19	94.7	76.2	9	133.7	107.6	19	110.4	88.8	12

[a] Frequencies and intensities computed with 6-311++G(3df, 3pd) are for harmonic calculations except where otherwise noted, and the SDD core potential and basis set are used for La. Intensities are calculated with B3LYP. Frequencies and intensities are in cm^{-1} and km/mol. CH_2-LaH_2 has a C_s structure with two equal La−H bonds at all levels of calculation performed in this study including CCSD/6-311++G(2d,p)/SDD. The symmetry notations are based on the C_s structure with two equal La−H bonds. [b] Calculated anharmonic frequencies.

CH_2D_2, and the observed frequencies are listed in Table 7. Both the **i** and **m** absorptions increased slightly upon visible irradiation, but increased markedly upon UV irradiation. Particularly in the CD_4 spectrum, they increased more than 10-fold upon UV irradiation. The original lower yields in the reaction of laser-ablated La with CD_4 can be traced to the lower deuterium tunneling rate caused by the smaller zero-point energy in the reaction path of C−D insertion. The original, low product concentrations of the deuterated products lead to the relatively high increases upon UV photolysis. Hydrogen stretching absorptions of LaH, LaH_4^-, and LaD_4^- are also observed at 1344.1, 1114.3, and 796.7 cm^{-1} in the IR spectra.[28]

Although the **i** absorption in the La−H stretching region of the La + CH_4 spectra is overlapped by a strong methane precursor absorption, as shown in Figure 6, the **i** La−H stretching absorption is observed at 1294.8 cm^{-1} in the CH_2D_2 spectra instead in Figure 8, and the deuterium counterpart is observed at 926.3 cm^{-1} (H/D ratio of 1.398). This absorption may be compared to the La−H stretching bands of LaH at 1344.1 cm^{-1} and LaH_2 at 1320.9 and 1283.0 cm^{-1}.[28] The La−H stretching band indicates that some C−H insertion product (CH_3-LaH) is formed in the reaction of La with CH_4 and visible photolysis, but mostly upon following UV irradiation. Another **i** absorption at 1083.5 cm^{-1} has its D and ^{13}C counterparts at 825.2 and 1074.2 cm^{-1} (H/D and $^{12}C/^{13}C$ ratios of 1.313 and 1.009), and it is attributed to the CH_3 deformation mode on the basis of the frequency and isotopic shifts.

The **m** absorption at 1246.8 cm^{-1} has its deuterium counterpart at 892.9 cm^{-1} but shows no ^{13}C shift, indicating that it is also a La−H stretching band. Evidently the higher frequency component of the hydrogen stretching pair is overlapped by a precursor absorption; however, its deuterium counterpart is barely discernible at 924.5 cm^{-1} on the edge of the stronger **i** absorption at 926.3 cm^{-1} in Figure 7. On the basis of its relatively lower La−H stretching frequency and isotopic variations, the bands most likely originate from CH_2-LaH_2, in line with the Y and Sc cases. The LaH_2 stretching pair is probably overlapped by the stronger **i** and precursor absorptions at 1294.8 and 1232.1 cm^{-1}, respectively, whereas the LaD_2 stretching pair and the La−D stretching band of CHD−LaHD at the middle of them are still discernible in Figure 8. A weak **m** absorption at 499.7 cm^{-1} has its ^{13}C counterpart at 491.9 cm^{-1} (not shown) ($^{12}C/^{13}C$ ratio of 1.016). It is tentatively assigned without observation of the deuterium counterpart to the CH_2 wagging mode, which is coupled with the C−La stretching mode.

The calculated frequencies of the La insertion and methylidene hydride complexes listed in Tables 8 and 9 are within the agreement expected for DFT-computed frequencies[1−7,29] with the observed values in Table 7. The observed bands are in fact the ones predicted to be the strongest. The La methylidene hydride complex is predicted to have a C_s structure with two equal La−H bonds out of the CH_2M plane at all levels of calculation used in this study, including the CCSD calculation with 6-311++G(2d,p). The C_s structure is compared to the C_{2v}

Table 10. Geometrical Parameters and Physical Constants Calculated for the Reaction Products of Group 3 Metals with Methane[a]

parameter	CH_3-ScH	CH_3-YH	CH_3-LaH	CH_2-ScH_2	CH_2-YH_2	CH_2-LaH_2
$r(C-H_1)$	1.101	1.095	1.100	1.093	1.095	1.101
$r(C-H_2)$	1.095	1.098	1.102	1.093	1.095	1.101
$r(C-H_3)$	1.095	1.098	1.102			
$r(C-M)$	2.280	2.315	2.437	2.159	2.335	2.451
$r(M-H_3)$				1.818	1.991	2.115
$r(M-H_4)$	1.882	1.965	2.084	1.818	1.991	2.115
$r(M\cdots H_1)$	2.734	2.931	3.042	2.936	3.111	3.225
$\angle H_1CH_2$	105.8	106.8	107.2	108.4	107.3	107.7
$\angle H_2CH_3$	105.8	106.4	107.2			
$\angle CMH_3$				119.5	119.3	112.6
$\angle CMH_4$	124.8	116.0	111.5	119.5	119.3	112.6
$\angle H_3MH_4$				121.1	121.2	114.4
$\angle H_1CM$	102.2	113.6	113.2	125.8	126.3	126.1
$\angle H_2CM$	117.4	111.4	111.0	125.8	126.3	126.1
$\Phi(H_1CMH_3)$	−115.2	−120.6	−120.5	0.0	0.0	22.9
$\Phi(H_1CMH_4)$	0.0	0.0	0.0	180.0	180.0	154.0
mol. sym.	C_s	C_s	C_s	C_{2v}	C_{2v}	C_s
$Q(C)^b$	−0.58	−0.84	−0.48	−0.59	−0.82	−0.73
$Q(H_1)^b$	0.00	−0.03	0.06	0.03	−0.02	0.10
$Q(H_2)^b$	−0.06	−0.02	0.02	0.03	−0.02	0.10
$Q(H_3)^b$	−0.06	−0.02	0.02	−0.56	−0.60	−0.35
$Q(H_4)^b$	−0.55	−0.63	−0.38	−0.56	−0.60	−0.35
$Q(M)^b$	1.26	1.54	0.76	1.78	2.06	1.23
μ^c	5.33	1.37	3.24	0.96	0.94	4.59
state[d]	$^2A'$	$^2A'$	$^2A'$	$^2B_1$	$^2B1$	$^2A'$
ΔE^e	12.7	18.1	28.9	12.5	7.4	0.1

[a] Bond lengths and angles are in Å and deg. The molecular parameters are calculated with CCSD. 6-311++G(3df, 3pd) basis set is used for Sc and Y complexes, and a smaller basis (6-311++G(2d,p)) is used for the La complexes. [b] Mulliken atomic charge. [c] Molecular dipole moment in D. [d] Electronic state. [e] Binding energies in kcal/mol relative to M + CH_4. SDD core potential and basis set are used for Y and La, while all-electron basis is used for the other atoms including Sc.

structure of CH_2-ScH_2. Therefore, both calculation and experimental results show the Sc, Y, and La methylidene hydride complexes have two equal metal−hydrogen bonds, unlike group 4−6 metal methylidene hydride complexes.[4−6]

Clearly the La insertion product is produced far more relative to the product responsible for the **m** absorptions as compared to the Y or Sc cases. This indicates that the insertion complex becomes more favorable over the methylidene hydride complex with increasing atomic mass among the group 3 metals. The molecular parameters of the insertion and methylidene hydride complexes are listed in Table 10. Stabilization by the matrix is not considered in the calculations; the methylidene hydride complex is expected to be more stabilized in the matrix due to its metal atom being in a higher oxidation state. It is notable that on the basis of the calculated binding energies the insertion complex becomes more stable relative to the methylidene hydride complex in the order of Sc, Y, and La, consistent with the observed results shown in Figures 1−8. The insertion complex is relaxed and trapped less relative to the methylidene hydride complex in the Sc system (Figures 4 and 5), whereas the two primary products persist until the last stage of annealing in the Y system (Figures 1−3).

However, the previously studied group 4−6 metal systems have shown a reverse trend; the higher-oxidation products are more favored with heavier metals in the same group.[1−7] The primary products in reactions of the first-row transition metals are all single insertion complexes (CH_3-MX, X = H, F, Cl, Br, and I), and the higher oxidation-state products are later produced in the following photolysis. On the other hand, the major reaction products of the third-row transition metals are higher oxidation-state complexes, and the single insertion complexes are often not identified in the IR spectra.

The **h** absorptions, which increase on annealing and at high concentration, are again believed to arise from higher-order complexes, similar to the Y and Sc cases.

Reaction Mechanisms. Group 3 metal atoms excited by laser ablation or by arc lamp irradiation activate methane to form the methyl metal hydride complex, which can undergo α-H transfer to produce the methylidene dihydride complex, reaction 1. Visible irradiation tends to favor the methyl metal hydride, and UV irradiation promotes rearrangement to the higher energy methylidene dihydride complex.

$$M^* + CH_4 \rightarrow CH_3-MH \rightarrow CH_2-MH_2 \qquad (1)$$

Structure. The CCSD structures of the methyl and methylidene hydride complexes of group 3 metals are illustrated in Figure 9 and the molecular parameters listed in Table 10. The T1 diagnostic as defined by Lee and Taylor is <0.020 for these calculations, which suggests that multireference character is not a problem for these doublet ground electronic states.[30] Interestingly enough, the C−M bond lengths of the insertion and methylidene hydride complexes are comparable with each other, in contrast to those of the previously studied analogous products of group 4−6 metals.[1−7] Other levels of calculations also give similar results. The C−M bonds of the Y and La methylidene hydrides are in fact 0.020 and 0.014 Å longer than the corresponding methyl metal hydrides as shown in Figure 9, respectively. Figure 10 gives the C_s structures calculated for the related CH_3-YH_2 and $CH_2{=}YH_2^-$ complexes.

It is also notable that the C−Sc bond of CH_2-ScH_2 is still 0.121 Å shorter than that of CH_3-ScH, which may be compared to the C−Zr bond of $CH_2{=}ZrH_2$, which is 0.261 Å shorter than that of CH_3-ZrH.[4d] The CH_3-ScH complex has an extra electron on the Sc atom (spin density 0.99) after forming the σ-bonds, whereas the methylidene dihydride complex contains the extra electron mostly on the carbon atom spin density (0.93), but Sc contains spin density (0.12) from sharing with carbon.

(30) Lee, T. J.; Taylor, P. R. *Int. J. Quantum Chem. Symp.* **1989**, *23*, 199.

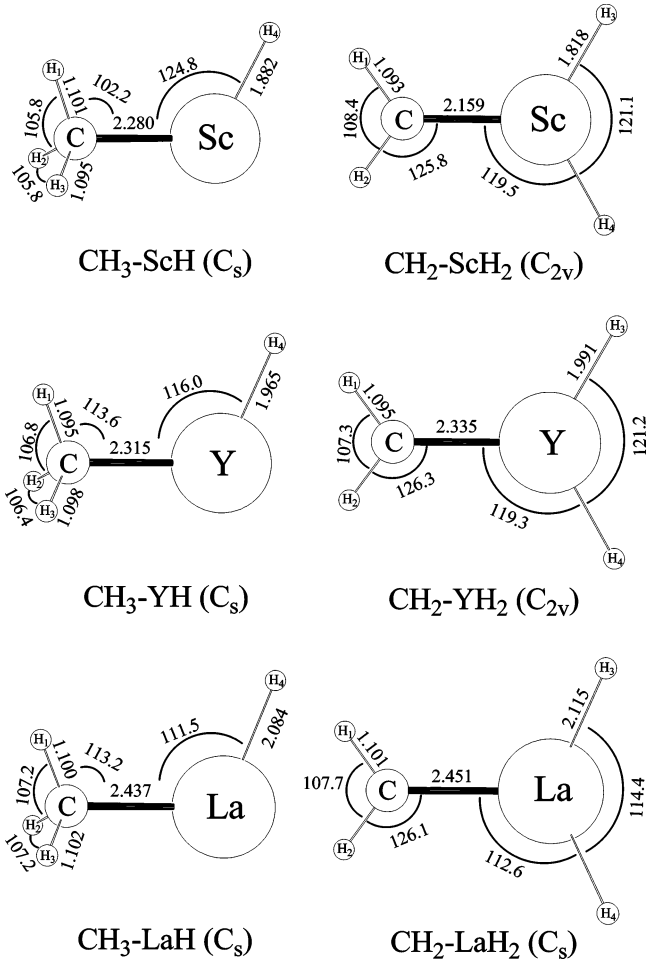

Figure 9. Optimized molecular structures of the methyl hydride and methylidene dihydride complexes of group 3 transition metals for the ground electronic state. The structures are calculated with CCSD/6-311++G(3df,3pd) for Sc and Y products and CCSD/6-311++G(2d,p) for La products. SDD core potential and basis set are used for the metals. CH_2-ScH_2 and CH_2-LaH_2 possess C_{2v} and C_s structures at all levels of theory used in this study, respectively, whereas CH_2-YH_2 has a C_s structure with B3LYP and BPW91 and a C_{2v} structure with MP2 and CCSD. The bond lengths and angles are in Å and deg.

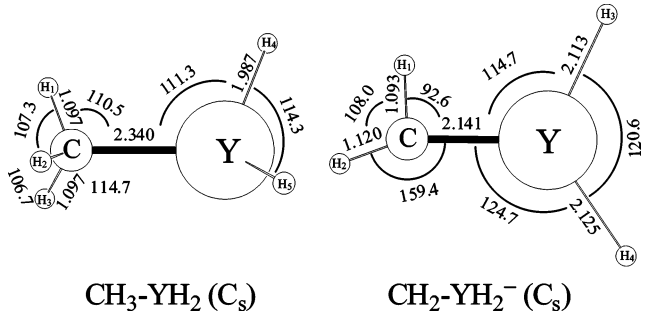

Figure 10. Optimized molecular structures of the methyl dihydride and methylidene dihydride anion complexes of yittrium. The structures are calculated with B3LYP and the 6-311++G(3df,3pd) basis set.

The present results indicate that donation of the extra electron to the vacant 3d-orbital of the Sc atom is relatively more effective than in the larger group 3 metal methylidene systems, giving more π-characteristics to the methylidene C−Sc bond than in the C−Y and C−La cases, where the C−M atomic spin density pairs are 0.96, 0.09 and 0.96, 0.08, respectively, from B3LYP/SDD (metal) computations.

Recent studies of metal reactions with CH_4 and CH_3X have shown that a shorter methylidene C−M bond normally leads to more agostic distortion.[1−7] The C−M bonds of the group 3 metal methylidenes are the longest among those of the early transition metal methylidenes. The symmetric methylidene hydride structures with the two equal M−H bonds are unique in comparison with the distorted structures of the previously studied group 4−6 metal methylidene hydrides prepared in reaction with CH_4 and CH_3X (X = F, Cl, Br, and I).[1−7,31]

The previous results also show that the electron density in the carbon−metal bond plays an important role in the magnitude of the distortion. Particularly in the CH_2-MHX systems, the distortion clearly increases with moving from left to right (from group 4 to group 6) in the periodic table.[1−3] The distortion also increases with increasing halogen size, probably by leaving more electron density in the C−M bond.

The C−M bond of the methylidene complex is essentially a single bond due to the small number of valence electrons of group 3 metals, and lack of significant π-electron density in the carbon−metal bond most likely results in a too small agostic interaction to cause distortion in the structure. The present and previous results reveal that the number of valence electrons of the metal atom is a crucial factor to determine the magnitude of the agostic interaction in the small methylidene complexes.[1−7] McGrady and Scherer reported that the agostic interaction is in fact delocalization of the carbon−metal bonding electrons,[32] implying that the electron density in the bond is a determining factor. Further theoretical as well as experimental studies are obviously necessary to examine the dramatic variation in the structures of small methylidene complexes with the number of valence electrons of the metal atom and the ligand electronegativity.

Conclusions

Methane activation was carried out with laser-ablated group 3 metal atoms, and the matrix infrared spectra of reaction products were investigated. Three sets of product absorptions marked "**i**, **m**, and **h**" are observed and grouped on the basis of the behaviors upon photolysis and annealing. The **i** and **m** absorptions increase markedly upon photolysis, while detailed variations depend on the metal. On the other hand, the **h** absorptions increase dramatically on annealing and at high concentration. They are attributed to the insertion of (CH_3-MH), methylidene dihydride (CH_2-MH_2), and higher-order methane complexes, respectively.

Results show that the insertion complex becomes relatively more favored with increasing atomic mass of the metal atom, a reverse to the general trend observed from previously studied group 4−6 metal systems.[1−7] The C−M bond length in CH_2-MH_2 is comparable to that of CH_3-MH, indicating that it is essentially a single bond, although small spin density is found on the metal center. This is in contrast to the $CH_2{=}MHX$ complexes formed with groups 4−6.[1−7] There is a parallel here with the observation of important group 4 $L_nM{=}NR$ species[33,34] and the recent failure to produce a scandium analogue.[35] Interestingly enough, the group 3 methylidene hydride com-

(31) von Frantzius, G.; Streubel, R.; Brandhorst, K.; Grunenberg, J. *Organometallics* **2006**, *25*, 118.
(32) Scherer, W.; McGrady, G. S. *Angew. Chem., Int. Ed.* **2004**, *43*, 1782.
(33) Hoyt, H. M.; Michael, F. E.; Bergman, R. G. *J. Am. Chem. Soc.* **2004**, *126*, 1018.
(34) Bytschkov, I.; Doye, S. *Eur. J. Org. Chem.* **2003**, 935.
(35) Knight, L. K.; Piers, W. E.; McDonald. R. *Organometallics* **2006**, *25*, 3289.

plexes are not agostically distorted, clearly different from the methylidene complexes of group 4−6 methylidenes.[1−7] The present results show that among the small early transition metal methylidene complexes, more valence electrons of the metal apparently lead to more agostic distortion. Group 3 methylidene complexes appear to be more reactive than their group 4 analogues, which may lead to applications for the development of catalyst systems.

Acknowledgment. We gratefully acknowledge financial support from NSF Grant CHE 03-52487 to L.A.

OM060816U